MANTECH Publications

Journal of Thermal Engineering and Technology

Volume 6 Issue 1

Review on Heat Transfer Enhancement using Advanced Enhancers

Zahid Ahsan[1], Umme Habiba[2], Mohammad Zoynal Abedin[3*]

Student[1, 2], Professor[3]

Department of Mechanical Engineering

Dhaka University of Engineering and Technology, Gazipur 1700, Bangladesh

Corresponding Authors' Email id: *- zahidahsan.93@gmail.com[1], habiba.me2011@gmail.com[2], abedin.mzoynal@duet.ac.bd[3]*

Abstract

This paper is another hopeful attempt to explore some of the phenomena observed in heat transfer enhancement by advanced heat transfer enhancers. Here it is reviewed the research work on heat transfer growth in advanced enhancers such as in fins and micro-fins, porous media, nanofluids, flexible seals, flexible complex seals, vortex generators, protrusions and ultra-high thermal conductivity composite materials heat exchangers. It illuminates the application of enhanced heat transfer surfaces as well. In this paper, it has been discussed on theoretical enhancement factors accompanying many heat transfer correlations for each enhancer. Furthermore, the effects of heat transfer enhancement and their applicability on the extended surfaces are also illustrated in this paper. Therefore, it is conjectured that the heat transfer has been tweaked night on 200% (2.0 times) for fins inside tubes when correlated with a smooth tube, 350% (3.5 times) for nanofluids when compared with normal fluid, 600% (6.0 times) for ultra-high thermal conductivity composite materials when analyzed with regular material and 1200% (12.0 times) in porous media when contrasted with general media.

Keywords*: - Internally finned tubes, Compound heat transfer enhancement, Nanofluids, Seals, Enhancement of heat transfer*

NOMENCLATURE

K permeability of the porous substrate
Nu Nusselt number
c_p fluid heat capacity
Do reference half thin-film width
T module thickness
W rate of airflow
L channel length
Pr Prandtl number lcp/k

INTRODUCTION

The heat exchangers have a significant job in vitality stockpiling and recuperation. Enhancement of heat transfer is of crucial significance in numerous modern applications. These days, a critical number of thermal designing researchers are looking for new improving heat transfer strategies among surfaces and the encompassing liquid. Because of this reality, Bergles [1,2] arranged that improving warmth moves as dynamic or inactive strategies.

Those which require the outer capacity to keep up the improvement instrument are named dynamic techniques. Instances of dynamic upgrade strategies are well mixing the liquid or vibrating the surface [3].

It had been portrayed by Hagge and Junkhan [4] that different dynamic mechanical improving techniques can be utilized to upgrade heat move. Then again, the uninvolved upgrade techniques are those which don't need the outside capacity to continue the improvements' qualities.

In the most recent decades, critical exertion has been made to create heat transfer upgrade strategies to improve the general exhibition of warmth exchangers. Henceforth, it is important to expand the warmth move execution of enhancer types.

The enthusiasm for these procedures is intently attached to vitality costs and, with the current increment in vitality cost, it is normal that the warmth move improvement field will experience another development stage. A more effective warmth exchanger can diminish the size of the warmth exchanger, in this way decreasing the expenses related to both material and assembling of the warmth exchanger [5].

Improved warmth move can make heat exchangers littler and more vitality productive. Warmth move improvement procedures allude to various enhancers used to build the pace of warmth without

influencing a lot of the framework's general presentation.

MECHANISMS OF AUGMENTATION OF HEAT TRANSFER

Regular heat transfer liquids, in any case, are lacking for high warmth motion applications, for example, superconducting magnets, super-quick registering and high force microwave tubes because of limitations of their warm properties, for example, conductivity. Various examinations have been done in the previous not many decades, trying to create novel strategies for upgrading the warm exhibition of warmth move liquids. An ongoing creation named nanofluids can resolve a few disservices related to huge particles' suspensions [6].

This work is worried about the convective warmth move of suspensions of carbon nanotubes (CNTs nanofluids). The inspirations driving are:

a) No past examinations have been found in writing on the convective warmth move of CNTs nanofluids.

b) Very high warm conductivity of carbon nanotubes and thus the incredible potential for huge warmth move improvement (3000 W/mK for multi-walled CNTs [7] and 6000 W/mK for single-walled CNTs [8]).

c) There are irregularities in a couple of detailed investigations on the convective warmth move utilizing nanofluids [9-12].

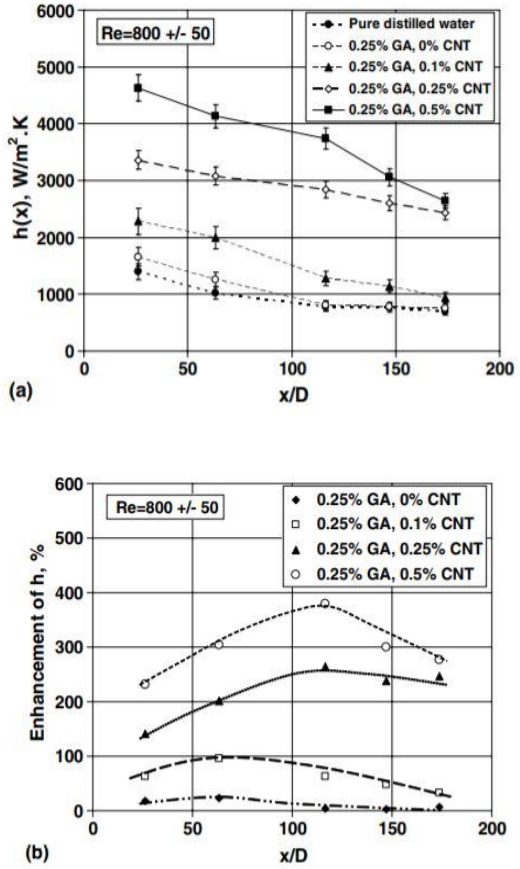

Figure 1: Axial Profiles of Heat Transfer Coefficient (a) and Enhancement of Heat Transfer Coefficient (b) for Different CNT Concentrations (Ph = ~6) [13].

Figure 1(a) shows the effect of CNT concentration on the local heat transfer coefficient at various axial distances from the entrance of the test section at Re =

800 ± 50 and pH = 6. Also included in the figure are the results of pure distilled water and gum Arabic– water solution for comparison purposes. Figure 1(b) shows the enhancement of the heat transfer coefficient, with reference to pure distilled water, as a function of axial distance at different CNT concentrations. The following observations can be made from the two figures:

- The presence of gum Arabic only gives a marginal enhancement on the heat transfer performance at x/D < 100, but the enhancement approaches to zero at x/D > 100 (Figure. 1a and b).

- The presence of carbon nanotubes increases the convective heat transfer coefficient significantly, and the increase is more considerable at high CNT concentrations (Figure. 1a).

- At a given CNT concentration, the heat transfer coefficient decreases with axial distance (Figure. 1a). This is as expected for heat transfer in the entrance region.

- The enhancement of heat transfer coefficient increases with x/D initially, reaches a maximum at a value of x/D depending on CNT concentration, and then decreases with a further increase in x/D. The value of x/D at which the enhancement is maximum increased with CNTs concentration (Figure 1b).

Figure 1(a) and (b) suggest a possible smart measure to keep the high heat transfer coefficient—creation of many artificial entrance regions along a pipeline. The use of artificial length will inevitably increase the pressure drop hence optimization is needed.

It had been showed by Ding et al., [13] that fluids containing 0.5wt.% of carbon nanotubes (CNT) can produce heat transfer enhancements over 250% at Re = 800, and the maximum enhancement occurs at an axial distance of approximately 110 times the tube diameter. The increases in heat transfer due to presence of nanofluids are thought to be associated with the following mechanisms.

a) Enhancing effective thermal conductivity of the fluid under static conditions.

b) Enhancing effective thermal conductivity of the fluid under dynamic conditions.

c) Delaying the boundary layer development.

d) Thermal dispersion.

e) Increasing the order of the fluid molecules.

f) Redistribution of the flow.

HEAT TRANSFER ENHANCERS

The heat transfer coefficient improvement capacity close to a base misfortune in contact factor characterizes the thermohydraulic execution of an enhancer.

In this paper, the writing audits are arranged into broadened surfaces, including balances and micro fins, permeable media, nanofluids, adaptable seals, adaptable complex seals, vortex generators, bulges, and ultra-high warm conductivity composite materials enhancers for getting distinctive heat transfer enhancement.

Heat Transfer Enhancement using Extended Surfaces (Fins)

Turbulent flow and heat transfer in finned tubes have been generally concentrated previously. The writing accessible on the exploratory examinations of fierce stream and warmth move in finned tubes is very broad.

One of the soonest trial chip away at the warmth move attributes of single-stage streams in inside finned tubes goes back to 1964 when it was introduced by Hilding and Coogan [14] that their information for ten diverse inner blade calculations for a 0.55 in. (14 mm) inward measurement copper tube with 0.01 in. (0.254 mm) straight metal balances utilizing air as the test liquid. It had been seen by Hilding and Coogan [14] that the warmth move is improved by around 100–200% over that of the smooth cylinder and the upgrade is joined by a comparative increment in the weight drop. The Reynolds number in this examination went from 1500 to 50,000.

Figure 2 shows the warmth move consequences of finned tube dependent on inside distance across and ostensible region as a component of Reynolds number and contrasts and that of smooth cylinder. The warmth move bend for finned tube is well over the smooth cylinder bend demonstrating upgrade of warmth move because of balances. Warmth move for the finned tube surpassed smooth cylinder esteems by 97% to 112% for Reynolds number range from 266000 to 786000.

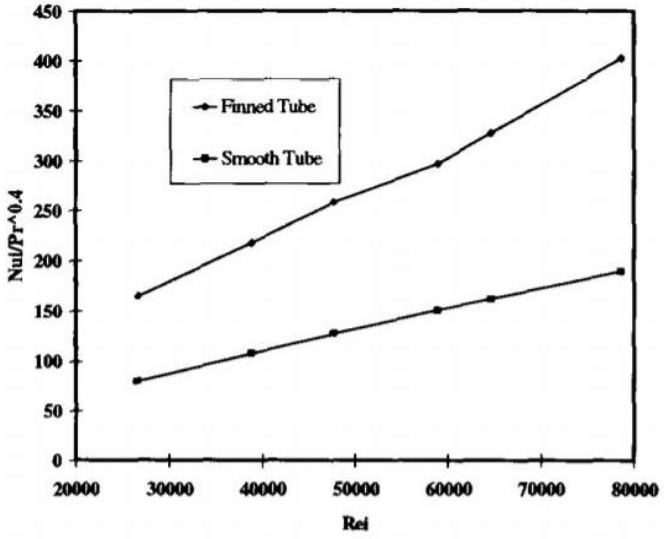

Figure 2: Variation of Nusselt Number Based on Inside Diameter and Nominal Area [15].

Most as of late, it has been tentatively controlled by Bharadwaj et al., [15] that warmth move attributes of fluid water streaming in a solitary 75 blade start spirally scored tube (inside distance across = 14.808 mm, f in helix point = 23◦, and f in stature = 0.3048 mm) with and without a turned tape embed. Results were introduced for uniform warming conditions at Pr = 5.4 in the range 300 < Re < 35, 000.

The scores are clockwise regarding the course of stream. It was noted by the creators that for the microfin tube tests change like qualities start at Re∼3000 and proceeded up to Re = 7000. Past this estimation of Re, the grinding factor remained almost steady like stream in an unpleasant cylinder. Force law-based relationship for the contact components and Nusselt numbers were introduced in the scopes of 300 < Re < 3000 (laminar), 3000 < Re < 7000 (change), and Re > 7000 (fierce).

It had been noticed that in the laminar and tempestuous scopes of Re, Nu is nearly multiplied contrasted with its incentive in a smooth cylinder as anticipated by the Dittus Boelter connection. Yet, for the change run 3000 < Re < 7000, the Nu-information nearly agree with a similar smooth cylinder relationship anticipated worth, demonstrating no improvement in heat move in this range. Consistent siphoning power correlation with smooth cylinder demonstrated that the spirally notched cylinder without wound tape yields greatest warmth move upgrade of 400% in the laminar range and 140% in the tempestuous range. Be that as it may,

for 2500 < Re < 9000, decrease in heat move was taken note.

The processed estimations of R for a winding cylinder without bent tape are plotted in Figure 3. It is seen that warmth move gain approaches almost 400% in the laminar range. Be that as it may, for 2500 < Resm < 9000, there is diminished warmth move. For Resm > 10,000, in any case, there is again an addition in heat move which lessens from 150% to 133% with increment in Resm. Figure 4 shows variety of R for spirally scored tube with turned tape.

The top figure shows brings about the laminar scope of Reynolds numbers. It is again observed that for all curve proportions, there is heat move improvement which changes from 160% to 600%. At turn proportion, Y = 10.14 and 3.4, anticlockwise curved tapes perform superior to clockwise tape. Yet, at Y = 7.95, the clockwise curved tape per frames superior to anticlockwise contorted tape.

This fascinating outcome comes from profoundly non-straight varieties of the f- and Nu-information in regard of bend proportion Y.

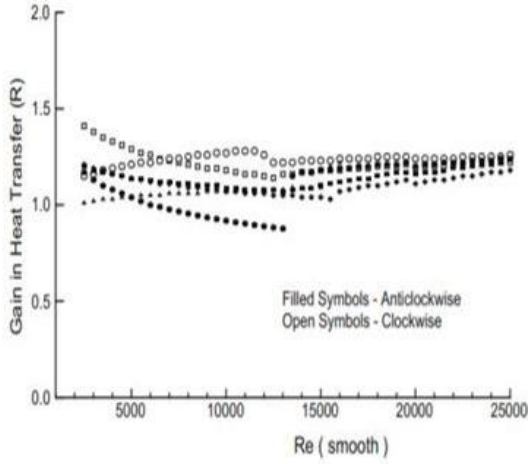

Figure 3: Heat Transfer Gain for Spirally Grooved Tube [15].

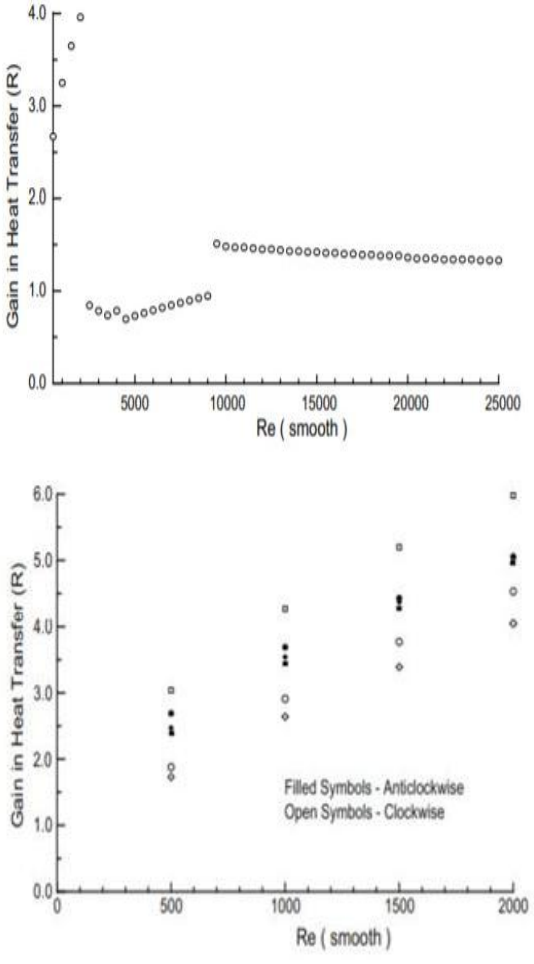

Figure 4: Heat transfer gain for grooved tube with twisted tape: Y = 10.15 (circles). Y = 7.95 (squares), Y = 3.4 (triangles) [15].

The above right side figure shows variety of R in the fierce range. Like the winding cylinder without a wound tape, at Y = 10.14 (most minimal contort) again disintegration in heat move is watched for 6000 < Resm < 13,000 for the anticlockwise turned tape. In the higher range (Resm > 13,000), However, again R > 1.

For the clockwise turned tapes high estimations of R are gotten at Y = 7.95 and 10.14. By and large, the clockwise wound tape performs better than the anticlockwise tape at all Reynolds numbers and Y. Generally speaking, at lower end of tempestuous Reynolds numbers (Resm=3000), most extreme addition is 140% at Y = 7.95. At better quality (Resm=25,000) most extreme addition of 133% at Y = 10.15 and 7.95 is demonstrated by the assessments.

In any case, a great part of the revealed information relates to huge blade frameworks. A large portion of the test relationships are pertinent just for the specific framework they were produced for.

It is additionally clear that many exact relationships dependent on test information do exist for anticipating heat move up to multiple times in tempestuous stream in finned tubes, yet it likewise appears to be that there is a considerable difference between the outcomes anticipated by these various connections; subsequently, a need exists for additional exploration here.

Heat Transfer Enhancement using Porous Media

Numerous works have been directed in the space of mostly fillings of permeable media. For instance, it had been led Jang and Chen [17] on a mathematical report for a constrained stream in an equal channel incompletely loaded up with a permeable medium by receiving the Darcy-Brinkman-Forchheimer model with a warm scattering term.

It had been introduced by Chikh et al. [18, 19] that a scientific answer for the completely evolved stream in annulus arrangement halfway loaded up with the permeable medium. It had been reached out by Al-Nimr and Alkam [20] that the investigations to the transient answer for annulus stream with the permeable layer.

They found that an expansion of up to multiple times in the Nu number was accounted for when annuli halfway loaded up with permeable substrates found either on the internal or the external chamber in

correlation with the reasonable annuli. It had been additionally researched by Alkam and Al-Nimr [21] that the warm presentation of an ordinary concentric cylinder heat exchanger by setting permeable substrates on the two sides of the inward chamber.

Mathematical outcomes indicated that permeable substrates of ideal thicknesses yield the greatest improvement in the warmth exchanger execution with moderate increment in the siphoning power. This kind of heat transfer enhancers is used in a wide range of practical applications, including (a) forced channel flow applications [22–26] and (b) renewable energy applications [24, 27]. Recent reviews of the subject are available in [16, 28].

Figures 5 and 6 show the axial velocity distribution in the radial direction at different axial locations, Z, for both cases I and O, respectively. These figures show that the mean liquid speed in the permeable area is lower than that free space. This is because of the extra hindrance of the stream brought about by the tiny inertial and gooey powers created by the permeable strong framework.

Additionally, the liquid mean speed in the permeable space diminishes as one walk downstream. The drafted fluid from the porous region enhances the fluid flow in the clear domain. It causes an increase in its maximum velocity and a simultaneous shift in the maximum velocity towards the porous layer, which is the source of the drafted fluid.

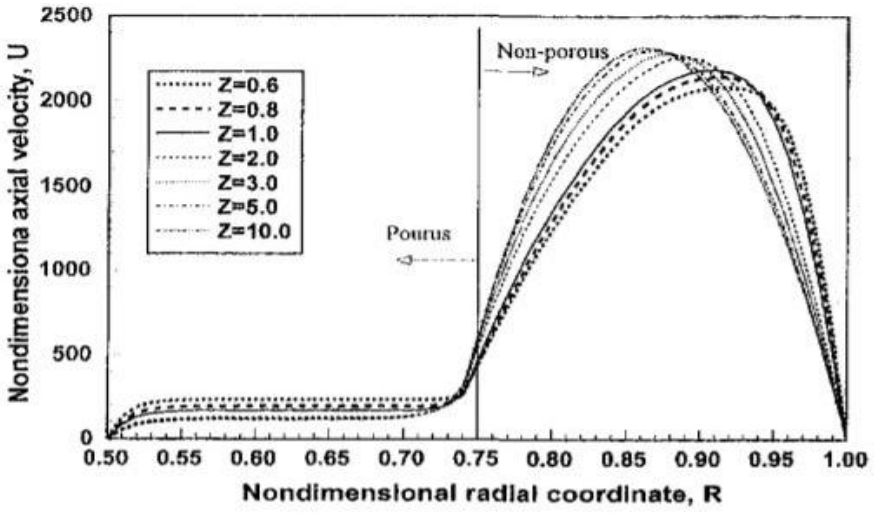

Figure 5: Non-Dimensional Axial Velocity Distribution in the Radial Direction at Different Axial Locations for Case I. A/2 = 0.75,4 = 10, and Da = 0.01 [20]

The effect of the microscopic inertial term (A) on the axial velocity radial distribution is shown in Figure 6. Increasing A implies an increase in the microscopic inertial retardation forces in the porous domain, and consequently, the fluid mean flow in the porous substrate decreases. On the other hand, the drafted fluid resulted from this retardation feeds the clear region and increases its mean velocity. Figure 7 shows the dynamic variation in the radial temperature distribution.

The figure suggests that external heating, which is applied on the outer cylinder, has more effective penetration (which is approximately 12 times) in the porous substrate than that in the clear fluid domain. This is due to the improvement in Nusselt number, as will be shown later.

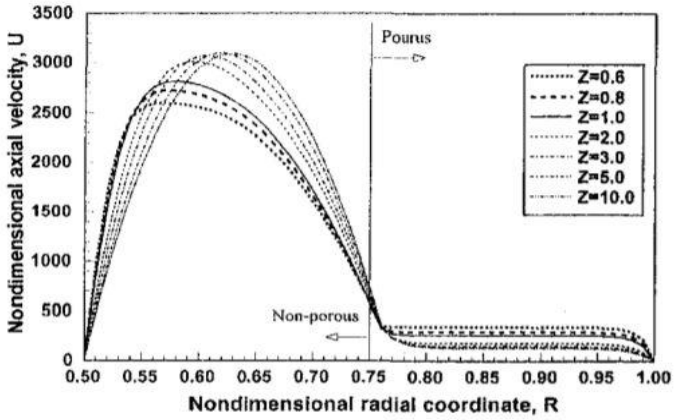

Figure 6: Non-Dimensional Axial Velocity Distribution in the Radial Direction at Different Axial Locations for Case O. A/2 = 0.75, 4 = 10, and Da = 0.01 [20].

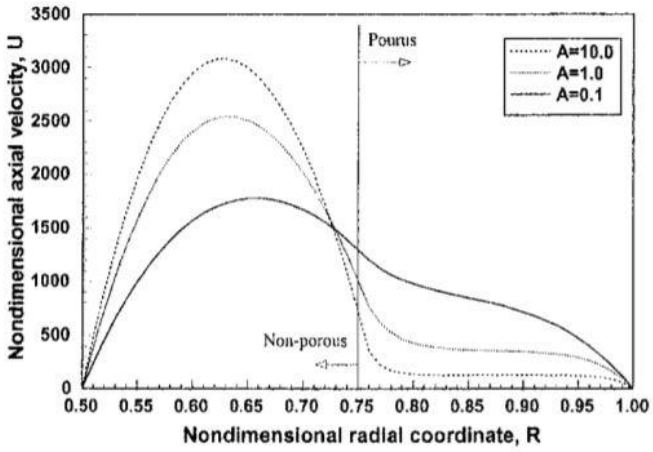

Figure 7: Non-dimensional Axial Velocity Distribution in the Radial Direction for Different Values of Forchheimer Number for Case O. Z = 10, W2 = 0.75 and Da = 0.1 [20].

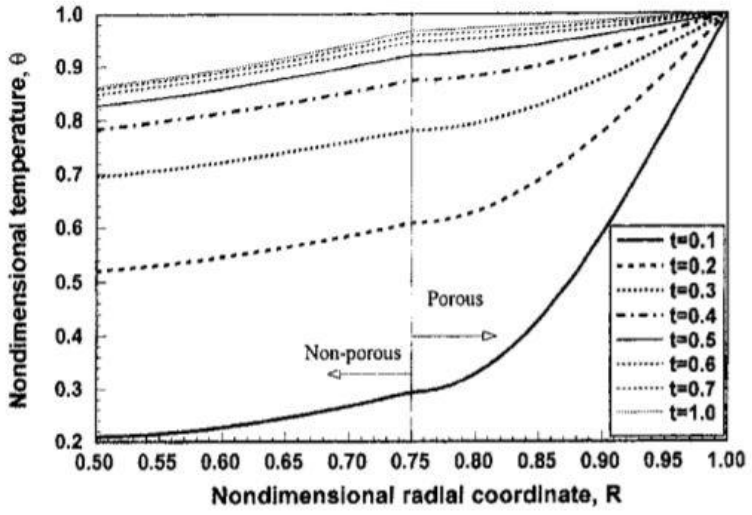

Figure 8: Non-dimensional Temperature Distribution in the Radial Direction for Different Times, at Z = 160 for Case O. W2 = 0.75, A = 10, And Da = 0.1 [20].

Heat Transfer Enhancement using Fluids with Large Particles Suspensions

An enormous number of examinations have been completed in the past to look for creating novel uninvolved strategies for improving the powerful warm conductivity of the liquid or expanding the convection heat move coefficient. One of the strategies is bringing into the base fluid high thermally conductive particulate solids, for example, metals or metal oxides. Instances of these examinations as per Ding et al. [6] are found in progress of Sohn and Chen [29], Ahuja [30, 31] and Hetsroni and Rozenblit [32].

These early examinations utilized suspensions of a millimeter or micrometer estimated particles. They gave some upgrades. Nonetheless, they acquainted issues with the warm framework such as scraped area and channel stopping up because of helpless suspension security, particularly on small or potentially miniaturized scale channels. Another inactive technique created by Choi [33] named "nanofluids" has appeared to determine a few detriments related to the suspensions of enormous particles.

Heat Transfer Enhancement using Nanofluids

Nanofluids are liquids that contain suspensions of nanoparticles of high thermally conductive materials like carbon, metals, and metal oxides into heat move liquids to improve the general warm conductivity. These nanoparticles are ordinarily of request 100 nm or less. Nanoparticles could be either circular or

barrel-shaped like carbon multiwalled nanotubes [34]. The benefits of appropriately built nanofluids, as per Ding et al. [6], incorporate the accompanying:

a) Higher warm conductivities than that anticipated by presently accessible naturally visible models,
b) Astounding security,
c) Little punishment because of an expansion in pressure drop, and
d) Little punishment because of an expansion in pipe divider scraped spot experienced by suspensions of a millimeter or micrometer particles.

It had been demonstrated by Ding et al. [6] that Xuan and Li [35] indicated that the convection heat move coefficient was expanded by ∼60% for a fluid-based nanofluid of 2% Cu nanoparticles by volume; however, the nanofluid just had a viable warm conductivity roughly 12.5% higher than that of the base fluid.

Additionally, they demonstrated that Wen and Ding [36] watched a ∼47% expansion in the convective warmth move coefficient of fluid c-alumina nanofluids at x/D ∼ 60 for 1.6 vol.% nanoparticles stacking and Re = 1600, which was a lot more noteworthy than that because of the upgrade of warm conduction (<~10%). Incredibly, It had been appeared by Ding et al. [6] that nanofluids containing 0.5 wt.% of carbon nanotubes (CNT) created an upgrade in convection heat move, which might be over 350% of that of the base fluid at Re = 800. The most extreme improvement happens at a hub separation of around multiple times the cylinder width.

This expansion is a lot more noteworthy than that because of the improvement of warm conduction (<~ 40%). The watched huge upgrade, which is 3.5 occasions than others of the convective warmth move coefficient is related with the accompanying reasons:

a) Upgrade of the warm conductivity under the static conditions,
b) Further upgrade on the warm conduction under the dynamic conditions (shear instigated),
c) Decrease of the limit layer thickness and deferral in the limit layer improvement,
d) Molecule re-plan due to non-uniform shear rate over the funnel cross-segment, and
e) High angle proportion of carbon nanotubes.

For nanofluids containing 0.5 wt.% CNTs, the most extreme upgrade comes to over

350% at Re = 800, which couldn't be ascribed simply to the improved warm conduction.

Heat Transfer Enhancement using Flexible Seals

Single layered (SL) and twofold layered (DL) microchannels upheld by adaptable seals are broke down in the progress of Vafai and Khaled [37]. In their work, the deformation of the supporting seals was related to the average internal pressure by the theory of elasticity. This relation is coupled with the momentum equation, which is solved numerically using an iterative implicit finite difference method. After solving these equations, they solved the energy equation. It had been showed that the cooling effect due to hydrodynamic expansion increases as the Prandtl number decreases. Further, the results show that SL flexible microchannel heat sinks mostly provide better cooling attributes compared to DL flexible microchannel heat sinks delivering the same coolant flow rate and having the same flexible seals. However, it had been indicated that unbending DL microchannel heat sinks give preferable cooling over inflexible SL microchannel heat sinks.

Later on, it had been discovered by Khaled [38] that the normal temperature of the warmed plate decreases as seals number (Fn) increases until Fn reaches an optimum, after which this temperature starts to increase with an increase in Fn.

Convective warmth move coefficient is diminished as F increments at low dimensionless weight drops, as appeared in Figure 9. This is on the grounds that coolant speeds decline close to the warmed plate as F increments. In that capacity, the convective warmth move coefficient increments as F increments for bigger Re0 and F esteems as delineated in Figure. 9.

Figure 10 shows that the mean mass temperature turns out to be less touchy to the dimensionless weight drop Re0 and the obsession boundary F as both F and Re0 increment.

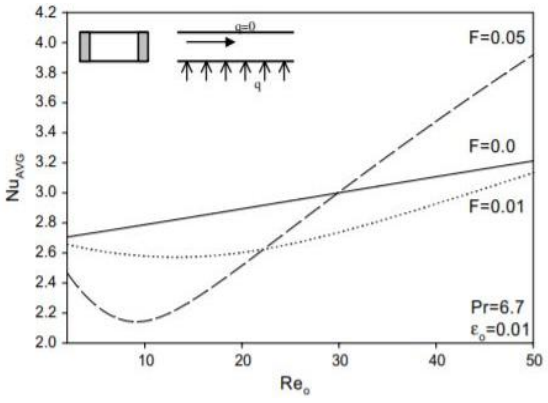

Figure 9: Effects of the Pressure Drop on the Dimensionless Average Convective Heat Transfer Coefficient for a Single Layer Flexible Microchannel Heat Sink [37].

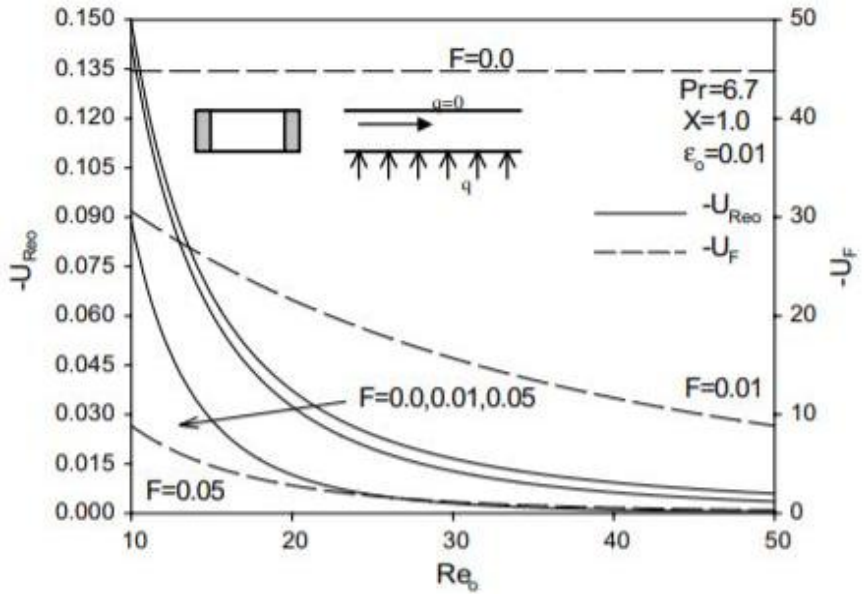

Figure 10: Effects of the Pressure Drop on Ure0 and Uf for a Single Layer Flexible Microchannel Heat Sink [37].

Figure 11 exhibits that adaptable microchannel heat sinks working at lower Reynolds numbers have lower warmed plate temperature at the exit as F increments. This isn't seen when these warmth sinks are worked at higher Reynolds number qualities.

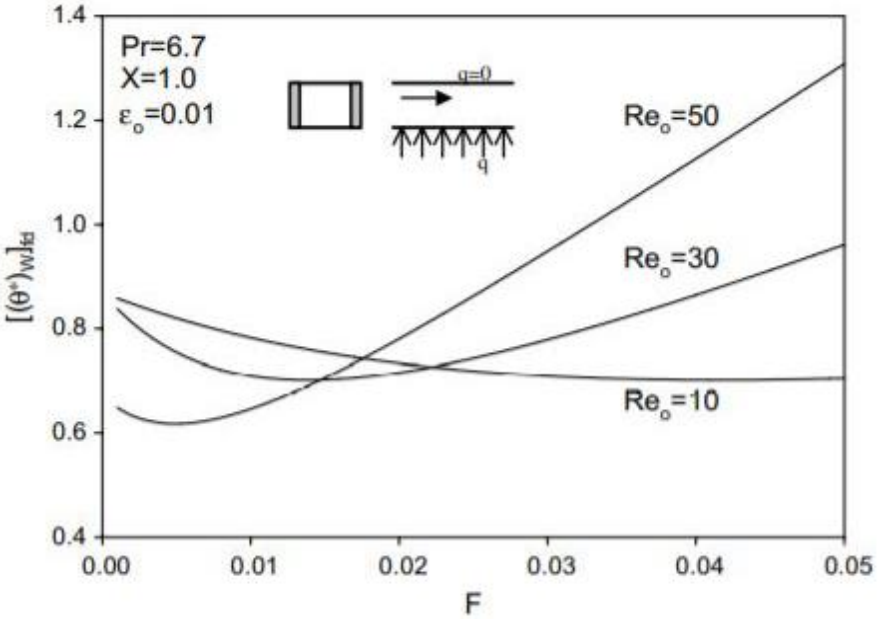

Figure 11: Effects of the Fixation Parameter on the Fully Developed Heated Plate Temperature at the Exit for a Single Layer Flexible Microchannel Heat Sink [37].

Figure 12 outlines the impacts of the obsession boundary F and Prandtl number Pr on the normal warmed plate temperature for SL adaptable microchannel heat sinks. As found in Figure. 9, adequate increment in the cooling impact can be accomplished by expanding F as Pr diminishes. This is predominantly because of an expansion in the coolant stream rate as F increments. Then again, convective warmth move coefficient is decreased as F increments at low Pr esteems as appeared in Figure 13. This is on the grounds that coolant speeds decline close to the warmed plate as F increments. As found in Figure 13, for huge Pr esteems, warm creating district impacts increment causing the convective warmth move coefficient to increment as F increments.

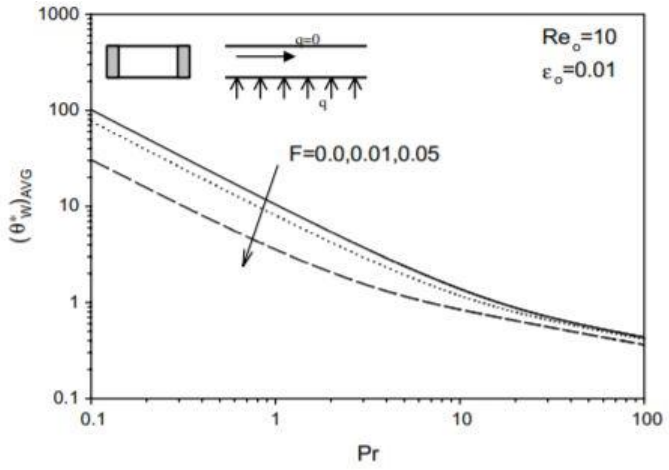

Figure 12: Effects of Prandtl Number on the Dimensionless Average Lower Plate Temperature For a Single Layer Flexible Microchannel Heat Sink [37].

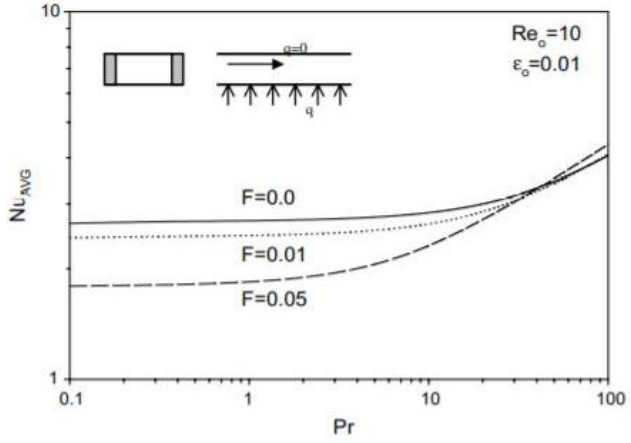

Figure 13: Effects of Prandtl Number on the Average Convective Heat Transfer Coefficient for a Single Layer Flexible Microchannel Heat Sink [37].

Figure 14 portrays the hub conduct of the mean mass temperature for two distinctive DL adaptable microchannel heat sinks having diverse obsession boundaries. Extra cooling is accomplished by presenting the auxiliary layer which can be found in Figure 14 for the case with F = 0.01. This plot shows that the greatest coolant temperature happens before the exit dissimilar to SL adaptable microchannel heat sinks where this temperature happens at the exit. As F builds, convection increments in the fundamental layer while conduction to the upper layer diminishes. This is because of an expansion in the convective warmth move and an expansion in the extension of the primary layer. Accordingly, the expansion in the cooling limit of DL adaptable microchannel heat sinks gets unimportant at both enormous estimations of the weight drop and the obsession boundary. This reality is unmistakably found in Figure 15 where the warmed plate temperature for DL adaptable microchannel heat sinks are nearly equivalent to that for the SL adaptable microchannel heat sinks with F = 0.05 for a wide scope of Re0. Note that jm is the proportion of the mean mass temperature at the exit for DL adaptable microchannel to that for SL adaptable microchannel heat sink. The boundary jW is the proportion of the normal warmed plate temperature for DL adaptable microchannel to that for SL adaptable microchannel heat sink.

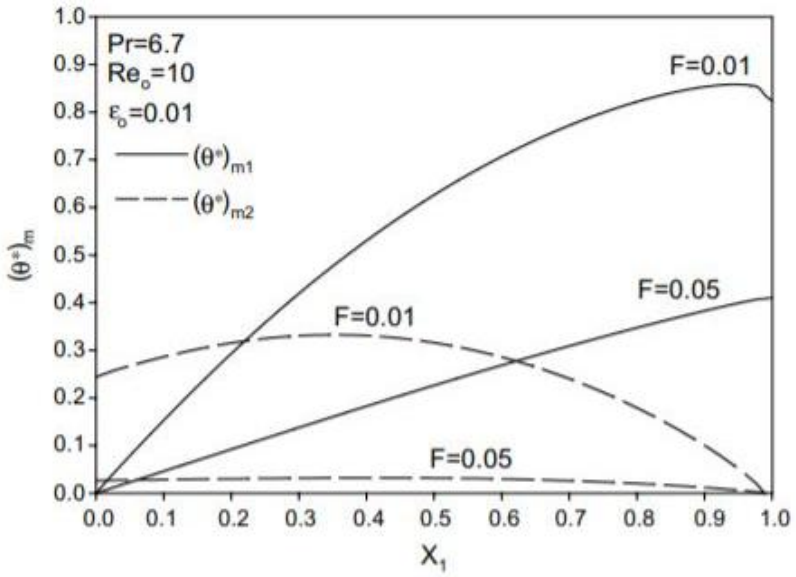

Figure 14: Effects of the Fixation Parameter on the Mean Bulk Temperature Inside the Double Layered Flexible Microchannel Heat Sink [37].

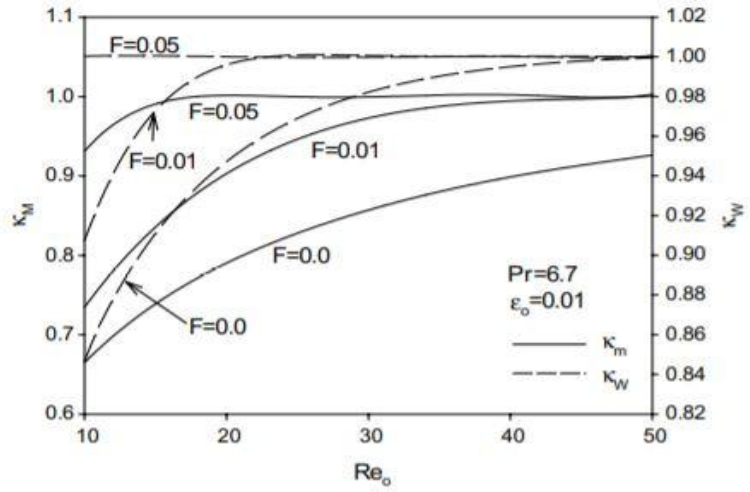

Figure 15: Effects of the Pressure Drop J_m And J_w [37].

Models for Heat Transfer Correlations using Flexible Seals and Flexible Complex Seals

It had been generated by Khaled and Vafai [39] that a correlation for normal Nusselt number (Nu)AVG and the dimensionless normal mean mass temperature for dainty movies upheld by adaptable complex seals with adaptable upper plates for the predefined scope of boundaries, $1.0 < S_1 < 10$, $1.0 < P_{e\varepsilon} < 50$ and $0 < F_{T1} < 1.0$.

He considered a fixed lower plate of the thin film while the upper plate is flexible and separated from the lower plate by soft complex seals that allow a local expansion in the thin film heights due to both changes in internal pressure and the lower (heated) plate temperature. Similar effects are expected when the upper plate is a bimaterial plate separated from the lower plate via soft seals.

The expansion in the local thin-film height and the lower plate temperatures decrease as the Peclet number Pe or the aspect ratio increase as shown in Figures 16 and 17, respectively. The decrease in H, m, and Pe as Pe increases is apparent when Pe <10. Figure 17 shows that the proposed cooling device can provide maximum enhancement in the cooling effect of 45% and above (compared to the performance ordinary flexible fluidic thin films) as the heating load increases when Pe is decreased below Pe = 0.5. This indicates that thermally expandable adaptable fluidic dainty movies are prescribed to be utilized in MEMS and electronic cooling applications. It is significant that expanding the warm extension boundary beyond certain values

will decrease the coolant velocity near the heated plate, which can result in a reduction in the cooling enhancement (as can be seen from Figure 18). This fact can also be seen from Figure 19, where the average Nusselt number decreases to a minimum and then increases as F_{T1} increases. For full and stable utilization of thermally expandable flexible fluidic thin films, the thermal expansion parameter is recommended to be lower.

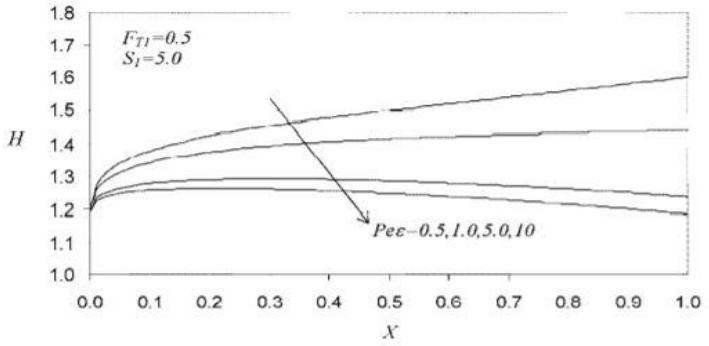

Figure 16: Variation of the Dimensionless Thin Film Height H with P_e (Category I) [39].

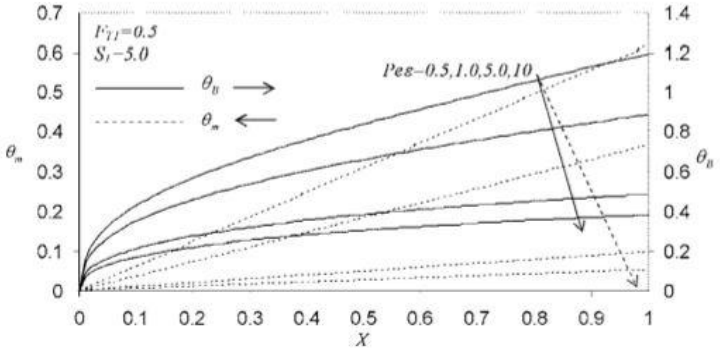

Figure 17: Variation of the Dimensionless Mean Bulk Temperature m and Dimensionless Lower Plate Temperature B With P_e (Category I) [39].

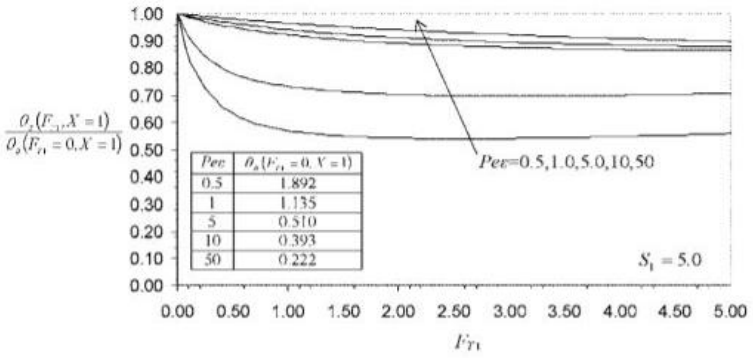

Pe	$\theta_o(F_{t1}=0, X=1)$
0.5	1.892
1	1.135
5	0.510
10	0.393
50	0.222

Figure 18: Variation of the Lower Plate Temperature at the Exit Relative to that when F_{t1}=0 with P_e and F_{t1} (Category I) [39].

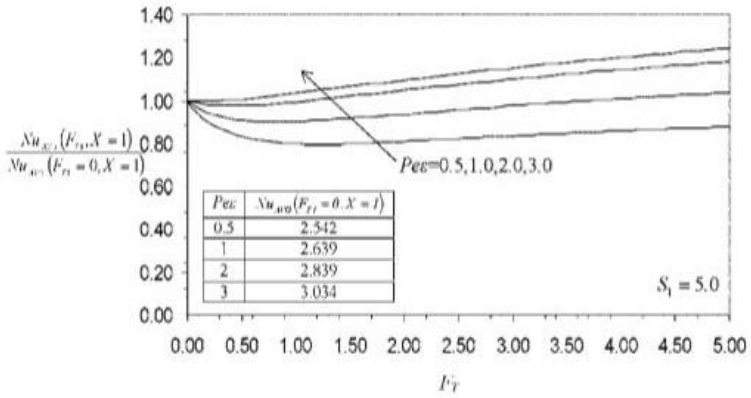

Figure 19: Variation of the Average Nusselt Number Nu_{avg} (F_{t1}, X =1) Relative to That When F_{t1}=0 with P_e and F_{t1} (Category I) [39].

The variation of the dimensionless is width D of the thin film with dimensionless axial distance X and the thermal expansion parameter F_{T2} for category II. It is noted that the thin film width increases as F_{T2} increases and that the maximum gradient of D occurs near the thin-film inlet. This increases normal stresses due to bending in this region. However, the increase in F_{T2} produces no insignificant cooling inside the thin film, as shown in Figure 20.

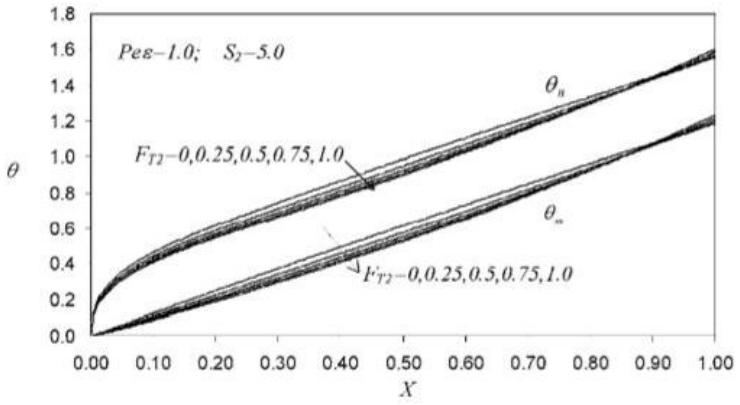

Figure 20: Variation of the Dimensionless Mean Bulk Temperature m and Dimensionless Lower Plate Temperature W with the Thermal Expansion Parameter F_{t2} (Category Ii) [39].

The coefficient is thermal expansion coefficient of the flexible complex seals. The boundary F_{T1} increments as the warming burden q, the warm development coefficient and the reference slim film stature increment while it diminishes as the liquid warm conductivity k diminishes. The solidness boundary S_1 is identified with the versatile properties of the adaptable complex seals.

Heat Transfer Enhancement using Vortex Generators

Figure 21 compares span-averaged Nusselt number distribution on the bottom wall in a channel for the case of a built-in circular tube, with and without winglet pair. The Nusselt number distribution starts with a high value and decreases in the flow direction due to the boundary layer's growth on the bottom plate. The Nusselt number assumes a high value near the axial location of the leading edge of the circular tube. As the fluid approaches the stagnation line of the circular tube, it slows down. The smaller velocity within the boundary layer in the vicinity of the bottom plate is here. Having impinged on the plate, the fluid rolls up, forming vortices that finally wrap around the front half of the tube and extend to the tube's rear [40]. The resulting motion can be best described as a horseshoe vortex system. The horseshoe vortices are also longitudinal vortices, and they promote disruption of the thermal boundary layer. The Nusselt number is enhanced due to the horseshoe vortices.

A sudden increase in Nusselt number is observed near the axial location of the winglet pair's trailing edges. Two counter-rotating longitudinal vortices culminate during the creation of a complex vortex system due to the winglet pair. The formation of longitudinal vortices brings about better mixing, and the Nusselt number becomes high near the winglets' location. The span-averaged Nusselt number reaches a high value (9.31) near the axial location of the leading edge of the circular tube. As already mentioned, this is primarily governed by the formation of the horseshoe vortices at the tube and bottom wall junction on the windward side. Up to the location of the leading edge of the winglet pair, the distribution of the span-averaged Nusselt number is the same for the cases with and without winglet pair.

However, beyond that location, the span-averaged Nusselt number increases for a channel with the tube and the winglet pair. The span-averaged Nusselt number's peak value takes place in the trailing edge neighborhood (X = 10.5) of the winglet pair, and its value is 10.74. The maximum enhancement in heat transfer (230%) is also observed at the same location. At the exit of the channel, the span-averaged Nusselt number is 6.03. The span-averaged Nusselt number at the exit of the plane channel is 4.22. The average Nusselt number value of the entire bottom plate for the case of a channel with a built-in circular tube and the winglet pair is 40% more than that for the case of a channel with a built-in circular tube.

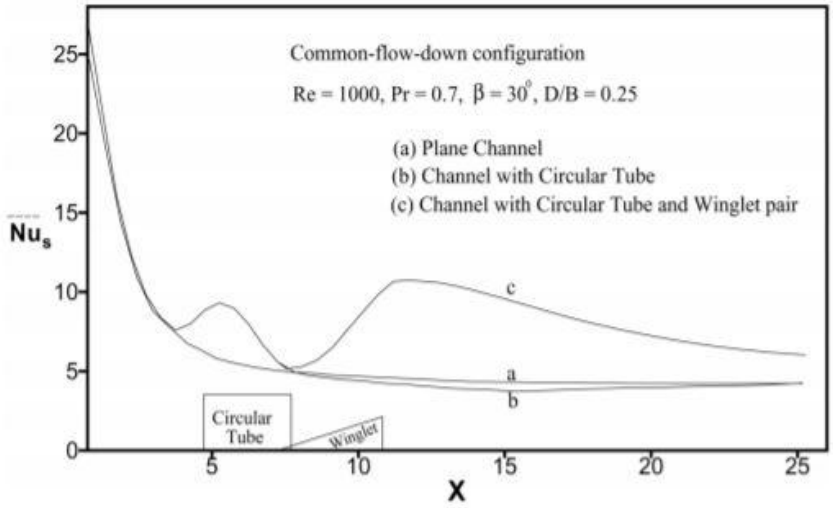

Figure 21: Distribution of Along Channel Length [40].

Figure 22 shows the distribution of local Nusselt number along the width of the channel at an axial location of X = 11. This location is in the immediate downstream of the trailing edge of the winglet pair. The flow field and the temperature field used for the calculation of local Nusselt number are at any arbitrary time instant. The peaks (Nu = 19.2) reconcile the effect of the counter-rotating longitudinal vortex pair. Maxima of the local Nusselt number occur at the span wise locations where the downwash due to vertical motions impinges on the bottom plate.

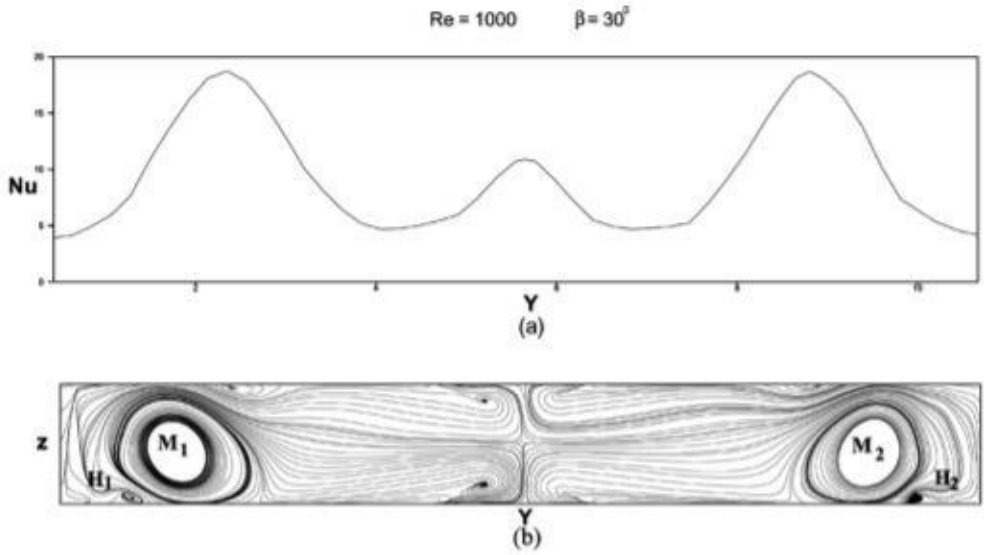

Figure 22: (a) Span-Wise Variation of Nusselt Number at X = 11. (b) Streamlines on the Cross Plane at Same Location [40].

Tiwari et al., [41] mathematically mimicked the impact of the delta winglet type vortex generator on the stream and warmth move in a rectangular conduit with an underlying round cylinder. They saw that the vortices prompted by the vortex generator brought about an expansion in the range arrived at the midpoint of Nusselt number at the following edge of the vortex generator by a factor of 2.5 and the warmth move upgrade of 230% in the close to wake district.

Heat Transfer Enhancement using Protrusions

The impact of rehashed flat bulges on the free-convection heat move in a vertical, lopsidedly warmed, channel has been tentatively examined by Tanda [45]. The bulges have a square segment and are made of a low warm conductivity material.

Analyses were directed by changing the quantity of the distensions over the warmed surface (whose stature was held fixed) and the angle proportion of the channel. The convective liquid was air and the divider to-encompassing air temperature contrast was set equivalent to 45 K. The nearby warmth move coefficient was acquired by methods for the schlieren optical procedure. The distensions were found to essentially modify the warmth move conveyance along the warmed surface of the channel, particularly in the region of every deterrent. For the scopes of boundaries considered, the expansion of low-conductivity distensions prompts a lessening in the normal warmth move coefficient, when contrasted with that for the smooth surface, in the 0–7% territory for the biggest divert viewpoint proportion and in the 18–43% for the littlest channel perspective proportion.

It had been directed by Saidi and Sunden [46] that a mathematical examination of the prompt stream and warmth move has been completed for counterbalanced strip balance calculations in self supported oscillatory stream.

The investigation depends on the two dimensional arrangement of the administering conditions of the liquid stream and warmth move with the guide of fitting computational liquid elements strategies. Shaky estimations have been done. The acquired time-subordinate outcomes are contrasted and past mathematical and test brings about terms of mean qualities, just as swaying attributes. The components of warmth move improvement are talked about and it has been demonstrated that the fluctuating temperature and speed second's display

non-zero qualities over the blades. The creation cycles of the temperature and speed changes have been considered and the uniqueness between these has been demonstrated.

It had been researched by Jubran et al., [47] that tentatively the impacts of rectangular and noncubical snags of different lengths, widths and statures on pressure drop and warmth move improvements. They found that adjustments in hindrance size or shape can prompt Nusselt number increments as stature as 40%. Sparrow et al. [43, 44] discovered that mass exchange upgrades of up to 100% can be acquired utilizing annoyances of uniform varieties of square obstructions.

A broad examination of the liquid and warmth move in an equal plate channel with a strong directing deterrent is led by Young and Vafai [42].

The rectangular deterrent was found to change the allegorical speed field fundamentally bringing about distribution zones both up-and downstream and a warm limit layer along the top face. Their outcomes show that the shape and material of the snag effectively affect the liquid stream and warmth move.

Exploratory outcomes will presently be accounted for the circumstance wherein there is both a boundary and a missing module in the cluster. Three classes of hindrance missing module arrangements were researched, and these are delineated in Figure 23.

In all cases, both the missing module and the monitored module are situated downstream of the barrier, since it has already been demonstrated that a barrier has virtually no effect on modules situated upstream of it. Correspondingly, as shown in Figure 23, the numbering system used to identify the rows of modules begins at the barrier. That is, the row immediately downstream of the barrier is row 1, the next is row 2, etc.

Table 1: K/K* and k/k* Ratios: Implanted Barriers and Missing Modules.

	A		B		C	
Row	2000	7000	2000	7000	2000	7000
1			1.66	1.65	1.58	1.53
2	2.16	1.97	1.98	1.87	2.03	1.93
3	1.99	1.78	1.67	1.59	1.73	1.61
4	1.68	1.60	1.50	1.43	1.50	1.48
5	1.57	1.53				
6	1.57	1.52				
7	1.55	1.53				
8	1.53	1.55				
9	1.51	1.47				
10	1.50	1.42				

Barrier height, $(b - t)/H = 2/5$.

Configurations Illustrated in Figure 23

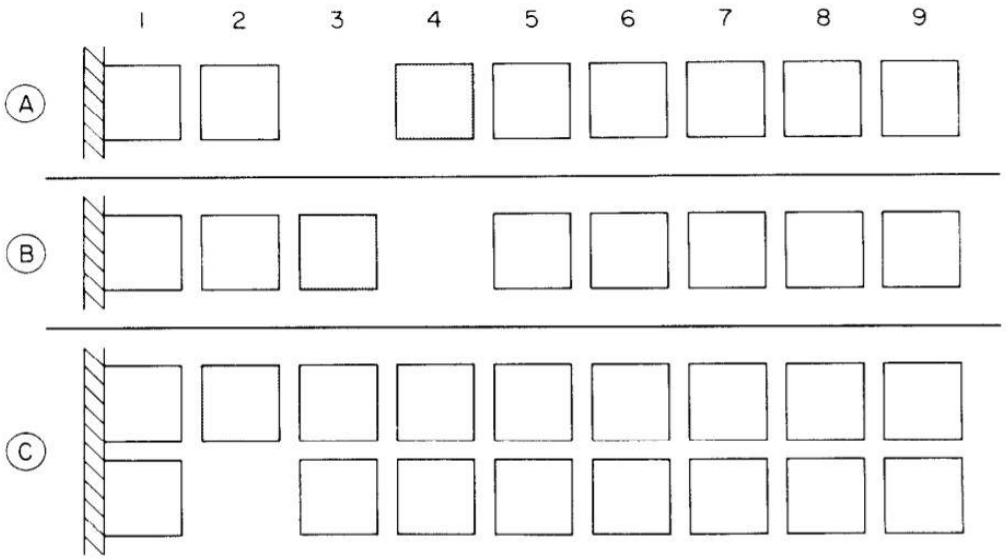

Figure 23: Categories of Barrier-Missing Module Configurations for which Experiments Were Performed [48, 49]

The three categories of barrier-missing module configurations are designated as A, B and C in Figure 23. In category A, the missing module is located immediately upstream of the speckled module at which the heat transfer characteristics are being monitored, whereas in category B the missing module is immediately downstream of the monitored module. In the third category, C, the missing module is just to the side of the monitored module.

The barrier implanted during this set of experiments is the taller of the two used in the experiments reported earlier in the paper. For this boundary, (b - t)/H = 3, that is, the obstruction squares 40% of the hole between the modules and the contrary divider. The hindrance was situated downstream of the passageway area.

Information runs were made for Reynolds numbers of 2OC0 and 7000. As before, the results are presented in terms of the K/K* and h/h* ratios. The numerator of the ratio is the value of the transfer coefficient at the monitored module when there is a barrier and a missing module in the array; the denominator represents the transfer coefficient for fully developed conditions in a fully populated array without barriers.

The K/K* and h/h* ratios are presented in Table 1 under columns A, B, and C which respectively correspond to the A, B and C categories of Figure 23. For each category, the results for the two Reynolds numbers

are listed side by side. In interpreting the tabulated information, it will be necessary only to focus on one of the Reynolds numbers, for instance, Re = 2000, since the same trends apply for both Reynolds numbers.

Consider first the results for category A. In this regard, it is useful to note that in the absence of a barrier, a missing module located just upstream of a monitored module gives rise to K/K* and h/h* ratios of 1.46 when Re = 2000. It is also useful to take note of the ratios listed in Fig. 7 for monitored modules situated downstream of a barrier. With this background, it may be seen from the second column of Table 1 that the separate enhancements due to a missing module and to a barrier are not directly additive when there is both a missing module and a barrier in the array.

However, the two effects are, in all cases, mutually reinforcing. Near the barrier, the already impressive barrier related enhancement is moderately increased due to the missing module. Well downstream of the obstruction, the classified proportions approach the worth 1.46 which relates to a missing module without hindrances.

For class B, it was discovered that in the close obstruction locale, a missing module situated downstream of the observed module has little impact on the K/K* and k/h* proportions which are incited by the boundary. A similar observation applies to a side-positioned missing module. The absence of added enhancement in the near barrier region, which is the region of interest when a barrier is implanted, prompted the truncation of the experiments after the fourth row.

Heat Transfer Enhancement using Ultra High Thermal Conductivity Composite Materials

Composite materials have been utilized fundamentally for basic applications. In any case, they have been discovered to be valuable for heat dispersal particularly in electronic gadgets. A case of such these materials is the metal framework composite (MMC). Commonplace MMCs that incorporates aluminum and copper lattice composites don't show significant upgrades in warm conductivity aside from while fortifying operator of fume developed carbon fiber (VGCF) is utilized as appeared in crafted by Ting and Lake [49].

For instance, VGCF-fortified aluminum network composite displays a warm conductivity that can be 642 W/mK with a

thickness of 2440 kg/m3 utilizing 36.5% of VGCF.

Nonetheless, all MMCs are electrically conductive. Chen and Teng [48] have demonstrated that VGCF tangle strengthened epoxy composites can have warm conductivities bigger 695 W/mK with thickness of 1480 kg/m3 what's more of having an electrically protecting surface.

This is with a fortification of 56% by volume of warmth treated VGCF. As of late, Naito et al. [50] have demonstrated that uniting of high warm conductivity carbon nanotubes (CNTs) is extremely powerful in improving the warm conductivity of specific kinds of carbon filaments, which can reach to 47% improvement.

Variety of warm conductivity in the X bearing with fiber volume portion is appeared in Figure 24 for all the 1D composites. Composite warm conductivity (filled circle) fundamentally observes the standard of blend.

For examination, hypothetical qualities determined utilizing 0.1 W/m K and 1950 W/m K for the warm conductivities of epoxy and VGCF, individually, are additionally appeared in Figure 24.

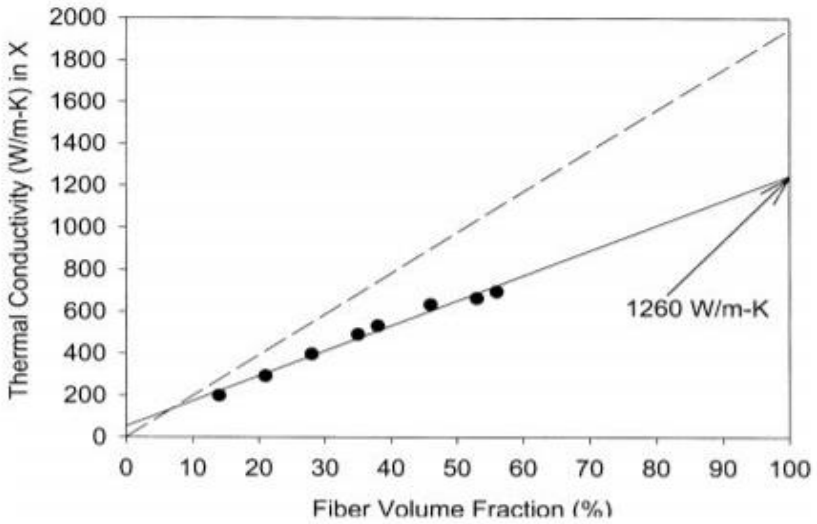

Figure 24: Thermal Conductivities (Filled Circles) of 1D Vgcf/Poly Mer Composites in the X (Primary) Direction. Solid Line is the Best Fit of the Data. Dashed Line Represents Theoretical Values Calculated Using Rule of Mixture With 0.1 W/m K and 1950 W/m K for the Matrix And Fiber Thermal Conductivities. [49].

Plainly the exploratory information are lower than hypothetical qualities, recommending a higher fiber warm conductivity was utilized in the hypothetical computations.

Extrapolation of the trial information gives a warm conductivity of ~1260 W/m K for the warmth treated VGCF. This is evidently much lower than 1950 W/m K, which was gotten by estimating a solitary fiber [51].

SUMMARY

Various methods are discussed with their outcomes in the paper. Some methods were applied experimentally and some were applied numerically in different mediums.

Also herewith mentioned heat transfer enhancement procedure which was investigated partially experimental and numerical ways. To figure out the effectiveness of each method to enhance heat transfer, it would be better to represent them in a table. A summary of heat transfer enhancement using various enhancers is shown in Table 2. Among various methods, it is found that porous media is more beneficial as it can enhance maximum heat transfer than other enhancers.

Advanced Enhancer	Enhancer Type	Observation	Reference
Fluids	Nanofluids	The heat transfer enhancement can be achieved as much as 350% (3.5 times) when compared with normal fluids.	**[6]**
Tubes	Fins inside tubes	The heat transfer enhancement can be achieved as much as 200% (2.0 times) when compared with smooth tubes.	**[14]**
	Micro-fins inside tubes	The heat transfer enhancement can be achieved as much as 400% (4.0 times) {for laminar flow} & 140% (1.4 times) {for turbulent flow} when compared with other enhancers.	**[15]**
Media	Porous media	The heat transfer enhancement can be achieved approximately 1200% (12.0 times) when compared with general media.	**[20]**
Seals	Flexible seals	The heat transfer enhancement can be achieved as much as 200% (2.0 times) when compared with other enhancers.	**[37]**
	Flexible complex seals	The heat transfer enhancement can be achieved as much as 300% (3.0 times) when compared with other enhancers.	**[39]**

Generator	Vortex generators	The heat transfer enhancement can be achieved as much as 250% (2.5 times) when compared with other enhancers.	**[41]**
Anatomical part	Protrusions	The heat transfer enhancement can be achieved as much as 200% (2.0 times) when compared with other enhancers.	**[43], [44]**
Composite materials	Ultra-high thermal conductivity composite materials	The heat transfer enhancement can be achieved as much as 600% (6.0 times) when compared with regular material.	**[48]**

Therefore, it is conjectured that the heat transfer has been improved as much as 200% (2.0 times) for fins inside tubes when compared with smooth tube, 350% (3.5 times) for nanofluids when compared with normal fluid, 600% (6.0 times) for ultra-high thermal conductivity composite materials when compared with regular material and 1200% (12.0 times) in porous media when compared with general media.

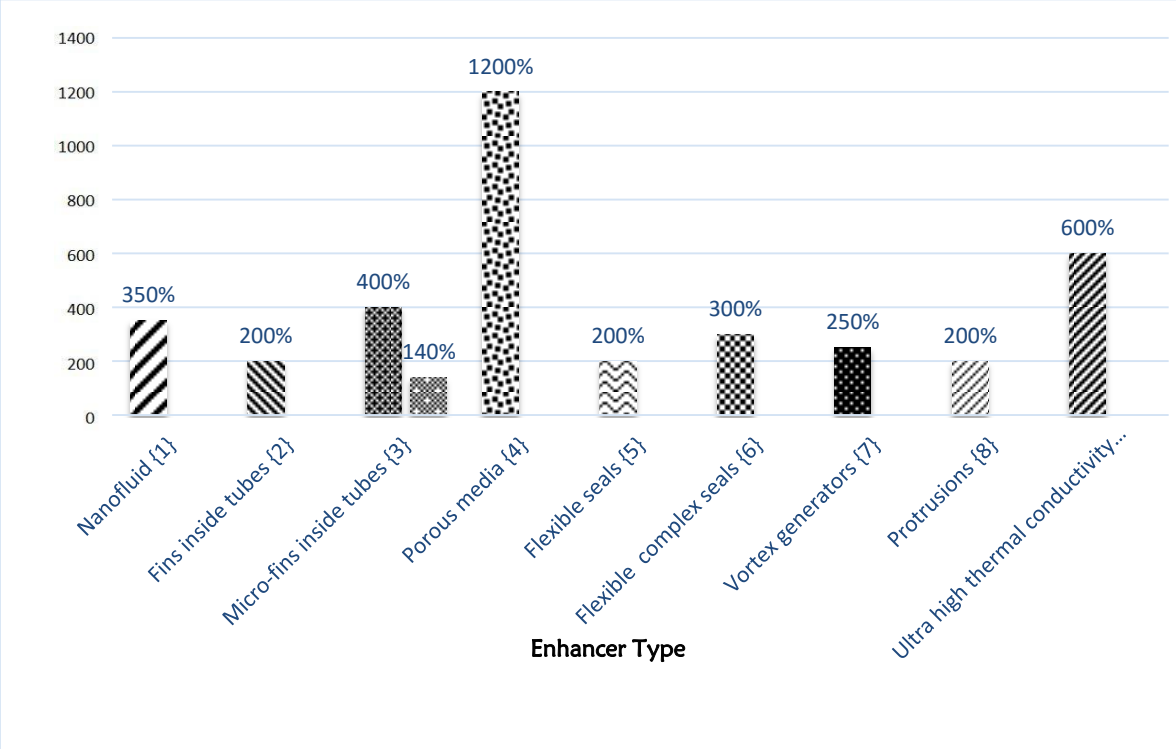

Figure 25: Percentage of Heat Transfer Enhancement against Advance Enhancers.

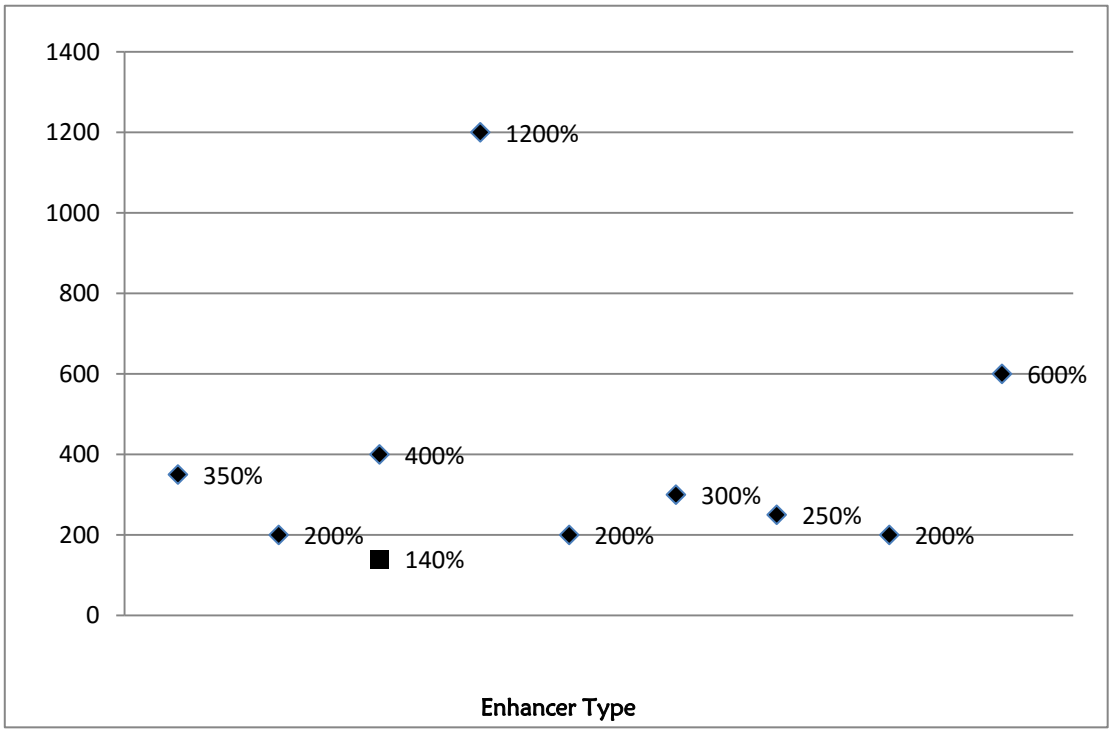

Figure 26: Comparative Representation of Heat Transfer Enhancement by Classified Enhancers.

Table 3: Estimated the Highest Recorded Heat Transfer Enhancement Level Due to Each Enhancer.

Sl. No.	Heat Transfer Enhancer Type	Heat Transfer Enhancement* [Reference]
{1}	Nanofluids	350% [6]
{2}	Fins inside tubes	200% [14]
{3}	Microfins inside tubes	400% for laminar [15] & 140% for turbulent [15]
{4}	Porous media	≈ 1200% (k_{eff}/k_f) [20]
{5}	Flexible seals	200% [37]
{6}	Flexible complex seals	300% [39]
{7}	Vortex generators	250% [41]
{8}	Protrusions	200% [43,44]
{9}	Ultra-high thermal conductivity composite materials	600% [48]

$$\textbf{* Heat transfer Enhancement} = \frac{\text{Heat transfer due to presence of the enhancer}}{\text{Heat transfer in absence of the enhancer}}$$

CONCLUSION

In this paper, the accompanying warmth move enhancers are depicted and evaluated: (a) extended surfaces including fins and micro fins, (b) porous media, (c) nanofluids, (d) flexible seals, (e) flexible complex seals, (f) vortex generators, (g) protrusions, and (h) ultra-high thermal conductivity composite materials. Different research works about each one have been reviewed, and many methods that assist their enhancement effects have been extracted from the literature.

It was concluded as follows: More consideration should be made towards single-stage heat move increased with micro fins to lighten the contradictions between crafted by the various creators.

Likewise, it was discovered that extra consideration ought to be made towards revealing the fundamental instruments of warmth move upgrades because of the nearness of nanofluids. In addition, we presumed that maybe the fruitful displaying of stream and warmth move inside permeable media, which is an all-around perceived latent improvement technique, could help in well finding the instrument of warmth move upgrades due to nanofluids. This is because of certain likenesses between both media. Furthermore, it is reasoned that perceptible considerations from analysts are required towards further demonstrating stream and warmth move inside convective media upheld by adaptable/adaptable complex seals so as to figure their degrees of warmth move upgrades.

Eventually, numerous ongoing works identified with inactive growths of warmth move utilizing vortex generators, distensions, and ultra-high warm conductivity composite material have been audited.

At long last, the assessed most extreme degrees of the warmth move improvement because of every enhancer are:-

1. The heat transfer enhancement can be achieved as much as 350% (3.5 times) when compared with normal fluids.

2. The heat transfer enhancement can be achieved as much as 200% (2.0 times) when compared with smooth tubes.

3. The heat transfer enhancement can be achieved as much as 400% (4.0 times) {for laminar flow} & 140% (1.4 times) {for turbulent flow} when compared with other enhancers.

4. The heat transfer enhancement can be achieved approximately 1200% (12.0 times) when compared with general media.

5. The heat transfer enhancement can be achieved as much as 200% (2.0 times) when compared with other enhancers.

6. The heat transfer enhancement can be achieved as much as 300% (3.0 times) when compared with other enhancers.

7. The heat transfer enhancement can be achieved as much as 250% (2.5 times) when compared with other enhancers.

8. The heat transfer enhancement can be achieved as much as 200% (2.0 times) when compared with other enhancers.

9. The heat transfer enhancement can be achieved as much as 600% (6.0 times) when compared with regular material.

ACKNOWLEDGEMENT

Supports from different academic and administrative personnel of Department of Mechanical Engineering, Dhaka University of Engineering & Technology (DUET) is greatly acknowledged.

REFERENCES

I. Bergles, A. E., Handbook of heat transfer. McGraw-Hill, New York, USA, 3rd edition, 1998.

II. E. Bergles, The implications and challenges of enhanced heat transfer for the chemical process industries. Chemical Engineering Research and Design, vol. 79, no. 4, pp. 437–444, 2001.

III. E. I. Nesis, A. F. Shatalov, and N. P. Karmatskii, Dependence of the heat transfer coefficient on the vibration amplitude and frequency of a vertical thin heater. Journal of Engineering Physics and Thermophysics, vol. 67, no. 1-2, pp. 696–698, 1994.

IV. J. K. Hagge and G. H. Junkhan, Experimental study of a method of mechanical augmentation of convective heat transfer in air. Tech. Rep. HTL3, ISU-ERI-Ames-74158, Iowa State University, Amsterdam, The Netherlands, 1975.

V. Leonard D. T., Pak, B. C., Baek, B. J., Dong Hwan Lee, A study on heat transfer enhancement using straight and twisted internal fin inserts. International Communications in Heat and

Mass Transfer. Vol. 33, pp. 719-726, 2006.

VI. Y. Ding, H. Alias, D. Wen, and R. A. Williams, Heat transfer of aqueous suspensions of carbon nanotubes (CNT nanofluids). International Journal of Heat and Mass Transfer, vol. 49, no. 1-2, pp. 240–250, 2006.

VII. P. Kim, L. Shi, A. Majumdar, P.L. McEuen, Thermal transport measurements of individual multiwalled nanotubes. Phys. Rev. Lett. 87 (21) 215502, 2001.

VIII. S. Berber, Y.K. Kwon, D. Tomanek, Unusually high thermal conductivity of carbon nanotubes. Phys. Rev. Lett. 84 4613–4616, 2000.

IX. B.C. Pak, Y.I. Cho, Hydrodynamic and heat transfer study of dispersed fluids with submicron metallic oxide particles. Experiment. Heat Transfer 11 151–170, 1999.

X. D.S. Wen, Y.L. Ding, Experimental investigation into convective heat transfer of nanofluids at entrance area under laminar flow region. Int. J. Heat Mass Transfer 47 (24) 5181–5188, 2004.

XI. Y.M. Xuan, Q. Li, Investigation on convective heat transfer and flow features of nanofluids. ASME J. Heat Transfer 125 151–155, 2003.

XII. Y. Yang, Z.G. Zhong, E.A. Grulke, W.B. Anderson, G. Wu,. Heat transfer properties of nanoparticle-in-fluid dispersion (nanofluids) in laminar flow. Int. J. Heat Mass Transfer 48 1107–1116, 2005.

XIII. Y. Ding, H. Alias, D. Wen, and R. A. Williams, Heat transfer of aqueous suspensions of carbon nanotubes (CNT nanofluids). International Journal of Heat and Mass Transfer, vol. 49, no. 1-2, pp. 240–250, 2006.

XIV. W. E. Hilding and C. H. Coogan, Heat transfer and pressure loss measurements in internally finned tubes. in Proceedings of ASME Symposium on Air Cooled Heat Exchangers, pp. 57– 85, 1964.

XV. P. Bharadwaj, A. D. Khondge, and A. W. Date, Heat transfer and pressure drop in a spirally grooved tube with twisted tape insert. International Journal of Heat and Mass Transfer, vol. 52, no. 7-8, pp. 1938–1944, 2009.

XVI. G. Lauriat and R. Ghafir, Forced convective transfer in porous media. in Handbook of Porous Media, K. Vafai and H. A. Hadim, Eds., Marcel Dekker, New York, USA, 2000.

XVII. J. Y. Jang and J. L. Chen, Forced convection in a parallel plate channel partially filled with a high porosity medium. International Communications in Heat and Mass Transfer, vol. 19, no. 2, pp. 263–273, 1992.

XVIII. S. Chikh, A. Boumedien, K. Bouhadef, and G. Lauriat, Analytical solution of non-Darcian forced convection in an annular duct partially filled with a porous medium. International Journal of Heat and Mass Transfer,

XIX. vol. 38, no. 9, pp. 1543–1551, 1995.

XX. S. Chikh, A. Boumedien, K. Bouhadef, and G. Lauriat, NonDarcian forced convection analysis in an annulus partially filled with a porous material. Numerical Heat Transfer A, vol. 28, no. 6, pp. 707–722, 1995.

XXI. M. A. Al-Nimr and M. K. Alkam, Unsteady non-Darcian forced convection analysis in an annulus partially filled with a porous material. Journal of Heat Transfer, vol. 119, no. 4, pp. 799–804, 1997.

XXII. M. K. Alkam and M. A. Al-Nimr, Improving the performance of double-pipe heat exchangers by using porous substrates. International Journal of Heat and Mass Transfer, vol. 42, no. 19, pp. 3609–3618, 1999.

XXIII. M. K. Alkam and M. A. Al-Nimr, Transient non-Darcian forced convection flow in a pipe partially filled with a porous material. International Journal of Heat and Mass Transfer, vol. 41, no. 2, pp. 347–356, 1998.

XXIV. M. A. Al-Nimr and M. K. Alkam, Unsteady non-Darcian fluid flow in parallel-plates channels partially filled with porous materials, Heat and Mass Transfer. vol. 33, no. 4, pp. 315–318, 1998.

XXV. M. A. Al-Nimr and M. K. Alkam, A modified tubeless solar collector partially filled with porous substrate. Renewable Energy, vol. 13, no. 2, pp. 165–173, 1998.

XXVI. M. K. Alkam, M. A. Al-Nimr, and M. O. Hamdan, On forced convection in channels partially

filled with porous substrates. Heat and Mass Transfer, vol. 38, no. 4-5, pp. 337– 342, 2002.

XXVII. M. O. Hamdan, M. A. Al-Nimr, and M. K. Alkam, Enhancing forced convection by inserting porous substrate in the core of a parallel-plate channel. International Journal of Numerical Methods for Heat and Fluid Flow, vol. 10, no. 5, pp. 502–517, 2000.

XXVIII. M. K. Alkam and M. A. Al-Nimr, Solar collectors with tubes partially filled with porous substrates, Journal of Solar Energy Engineering. vol. 121, no. 1, pp. 20–24, 1999.

XXIX. J. L. Lage and A. Narasimhan, Porous media enhanced forced convection fundamentals and applications. in Handbook of Porous Media, K. Vafai and H. A. Hadim, Eds., Marcel Dekker, New York, USA, 2000.

XXX. C. W. Sohn and M. M. Chen, Microconvective thermal conductivity in disperse two-phase mixtures as observed in a low velocity couette flow experiment. Journal of Heat Transfer, vol. 103, no. 1, pp. 47–51, 1981.

XXXI. A. S. Ahuja, Augmentation of heat transport in laminar flow of polystyrene suspensions. I. Experiments and results. Journal of Applied Physics, vol. 46, no. 8, pp. 3408–3416, 1975.

XXXII. S. Ahuja, Augmentation of heat transport in laminar flow of polystyrene suspensions. II. Analysis of the data. Journal of Applied Physics, vol. 46, no. 8, pp. 3417–3425, 1975.

XXXIII. G. Hetsroni and R. Rozenblit, Heat transfer to a liquid-solid mixture in a flume, International Journal of Multiphase Flow. vol. 20, no. 4, pp. 671–689, 1994.

XXXIV. S. U. S. Choi, Enhancing thermal conductivity of fluids with nanoparticles, in Developments Applications of NonNewtonian Flows. D. A. Siginer and H. P. Wang, Eds., vol. 231/MD-vol. 66, pp. 99–105, ASME, New York, USA, 1995.

XXXV. P. Garg, J. L. Alvarado, C. Marsh, T. A. Carlson, D. A. Kessler, and K. Annamalai, An experimental study on the effect of ultrasonication on viscosity and heat transfer performance of multi-wall carbon nanotube-based aqueous nanofluids. International Journal of Heat and Mass

Transfer, vol. 52, no. 21-22, pp. 5090–5101, 2009.

XXXVI. Y. Xuan and Q. Li, Investigation on convective heat transfer and flow features of nanofluids, Journal of Heat Transfer. vol. 125, no. 1, pp. 151–155, 2003.

XXXVII. D. Wen and Y. Ding, Experimental investigation into convective heat transfer of nanofluids at the entrance region under laminar flow conditions, International Journal of Heat and Mass Transfer. vol. 47, no. 24, pp. 5181–5188, 2004.

XXXVIII. K. Vafai and A.-R. A. Khaled, Analysis of flexible microchannel heat sink systems. International Journal of Heat and Mass Transfer, vol. 48, no. 9, pp. 1739–1746, 2005.

XXXIX. A.-R. A. Khaled, The role of expandable thermal systems in improving performance of thermal devices. International Journal of Thermal Sciences, vol. 46, no. 4, pp. 413–418, 2007.

XL. A.-R. A. Khaled and K. Vafai, Analysis of thermally expandable flexible fluidic thin-film channels. Journal of Heat Transfer, vol. 129, no. 7, pp. 813–818, 2007.

XLI. Goldstein, R.J. and Karni, J. The effect of a wall boundary layer on a local mass transfer from a cylinder in crossflowí. Journal of Heat Transfer (ASME), Vol. 106, pp. 260-267, 1984.

XLII. S. Tiwari, P. L. N. Prasad, and G. Biswas, A numerical study of heat transfer in fin-tube heat exchangers using winglettype vortex generators in common-flow down configuration. Progress in Computational Fluid Dynamics, vol. 3, no. 1, pp. 32–41, 2003.

XLIII. T. J. Young and K. Vafai, Convective cooling of a heated obstacle in a channel. International Journal of Heat and Mass Transfer, vol. 41, no. 20, pp. 3131–3148, 1998.

XLIV. E. M. Sparrow, J. E. Niethammer, and A. Chaboki, Heat transfer and pressure drop characteristics of arrays of rectangular modules encountered in electronic equipment. International Journal of Heat and Mass Transfer, vol. 25, no. 7, pp. 961–973, 1982.

XLV. E. M. Sparrow, A. A. Yanezmoreno, and D. R. Otis Jr., Convective heat transfer response to height differences in an array of block-like electronic components.

International Journal of Heat and Mass Transfer, vol. 27, no. 3, pp. 469–473, 1984.

XLVI. G. Tanda, Natural convective heat transfer in vertical channels with low-thermal-conductivity ribs. International Journal of Heat and Fluid Flow, vol. 29, no. 5, pp. 1319–1325, 2008.

XLVII. A. Saidi and B. Sunden, A numerical investigation of heat transfer enhancement in offset strip fin heat exchangers in self-sustained oscillatory flows. International Journal of Numerical Methods for Heat and Fluid Flow, vol. 11, no. 7, pp. 699–717, 2000.

XLVIII. A. A. Jubran, S. A. Swiety, and M. A. Hamdan, Convective heat transfer and pressure drop characteristics of various array configurations to simulate the cooling of electronic modules. International Journal of Heat and Mass Transfer, vol. 39, no. 16, pp. 3519–3529, 1996.

XLIX. Y.-M. Chen and J.-M. Ting, Ultra high thermal conductivity polymer composites. Carbon, vol. 40, no. 3, pp. 359–362, 2002.

L. J. Ting and M. L. Lake, Vapor grown carbon fiber reinforced aluminum composites with very high thermal conductivity. Journal of Materials Research, vol. 10, no. 2, pp. 247–250, 1995.

LI. K. Naito, J.-M. Yang, Y. Xu, and Y. Kagawa, Enhancing the thermal conductivity of polyacrylonitrile- and pitchbased carbon fibers by grafting carbon nanotubes on them. Carbon, vol. 48, no. 6, pp. 1849–1857, 2010.

LII. Heremans J, Beetz CP. J Phys, Rev 1985; B32:–5, 1981.